Acta Geophysica (2025) 73:3923–3942
https://doi.org/10.1007/s11600-025-01622-5

RESEARCH ARTICLE - SOLID EARTH SCIENCES

Analyzing the October 16, 2024 MW 5.9 Kale (Malatya) earthquake in relation to the February 2023 Kahramanmaraş earthquake sequence and local tectonic dynamics

Mustafa Senkaya[1,2] · Hamdi Alkan[3] · Serkan Öztürk[4] · Aydın Büyüksaraç[5]

Received: 16 November 2024 / Accepted: 14 May 2025 / Published online: 19 June 2025

Abstract

The 6 February 2023 Mw 7.7–7.6 Kahramanmaraş earthquake sequence has significantly impacted the East Anatolian Fault zone, including the city of Malatya and its immediate surroundings. In addition to the aftershocks of February 2023, the Mw 5.9 Kale earthquake that occurred on October 16, 2024, further underscores the ongoing seismic activity in the region. This study analyzes the distribution of *b*-values derived from a comprehensive dataset comprising 14,549 earthquakes and the Coulomb stress variations associated with the aftershocks of the February 2023 sequence and the Kale earthquake. The primary objective of this analysis is to enhance the understanding of the tectonic setting that contributed to the occurrence of the Kale earthquake. The findings indicate that the low *b*-values and stress transfer through the Pütürge segment toward the unnamed fault near Kale are significant contributing factors to the occurrence of the Kale earthquake. Additionally, positive stress variations from Doğanşehir to Malatya's city center suggest a potential fault oriented toward the city center that may increase the current earthquake hazard. Furthermore, the distribution of seismic events around Malatya suggests a possible barrier supported by previous magnetic data analysis between Malatya and Kale. Lastly, the observed stress variations for the Kale earthquake indicate the likelihood of upcoming seismic events in both the northeast and southwest directions of the Kale.

Keywords 2024 Kale earthquake · *b*-value distribution · Stress change · Local barrier

Introduction

The Anatolian Plate in the Alpine-Himalayan Mountain belt frequently attracts intensive attention from the earth scientists for its seismicity and tectonic activity. The westward motion (~25 mm/yr) and counterclockwise rotation of the Anatolian Plate are under the influence of the northward convergence of the Arabian Plate with a slip rate of ~15 mm/yr, the southward convergence of the Eurasian Plate with a slip rate of ~5 mm/yr and convergence of the African Plate in the south (Reilinger et al. 2006; Emre et al. 2018; Whitney et al. 2023; Ali and Abdelrahman 2023; Gabriel et al. 2023). The tectonic driving of the Anatolian Plate is along its major and complex boundary fault zones, right-lateral North Anatolian Fault Zone (NAFZ) and left-lateral East Anatolian Fault Zone (EAFZ). The EAFZ extends over 550 km in length from Karlıova Triple Junction (KTJ) in the northeast (NE) to the east (E) of Türkoğlu Basin and Amik Triple Junction in the southwest intersected Dead Sea Fault Zone (DSFZ) (Karabacak et al. 2023; Alkan et al. 2024; Yolsal-Çevikbilen et al. 2024). The EAFZ consists of many distinct strands, conjugate fractures, pull-apart basins, and main segments that produced significant/destructive earthquakes in instrumental and historical periods (Emre et al. 2018; Li et al. 2023). Bayrak et al. (2015) investigated the earthquake hazard of the EAFZ by determining the a and b

Edited by Dr. Rodolfo Console (ASSOCIATE EDITOR) / Prof. Ramón Zúñiga (CO-EDITOR-IN-CHIEF).

✉ Mustafa Senkaya
mustafasenkaya@uludag.edu.tr

1 Department of Civil Engineering, Bursa Uludağ University, TR-16240 Bursa, Turkey

2 Earthquake Research and Structural Health Monitoring Laboratory, Bursa Uludağ University, TR-16240 Bursa, Turkey

3 Department of Geophysics, Van Yüzüncü Yıl University, TR-65080 Van, Turkey

4 Department of Geophysics, Gümüşhane University, TR-29100 Gümüşhane, Turkey

5 Can Vocational School, Çanakkale Onsekiz Mart University, TR-17400 Çanakkale, Turkey

parameters in the Gutenberg-Richter magnitude-frequency relationship by dividing the EAFZ into five different source lines according to their tectonic and seismotectonic regimes. Accordingly, they obtained the lowest b value covering the Karlıova triple junction. The last and most important of these devastating earthquakes, on 6 February 2023, a destructive doublet earthquake ($M_W = 7.7$ and $M_W = 7.6$) occurred in Narlı-Pazarcık and Ekinözü-Elbistan (Kahramanmaraş). The earthquake with a magnitude of Mw 7.7 that occurred in the Pazarcık District of Kahramanmaraş in southern Turkey on February 6, 2023 significantly affected 11 provinces in southern Turkey and northern Syria (AFAD 2024a). Many aftershocks between Mw 5.0–6.0 were seen at various locations. Then, the second earthquake with a magnitude of Mw 7.6 that occurred 9 h later on the same day in Elbistan, northwest of Kahramanmaraş (AFAD 2024b), and had very severe effects in the settlements around Malatya discussed in this study. While, twenty-three aftershocks below MW 6.0 could be seen on region after second earthquake at various sites according to the Disaster and Emergency Management Presidency of Türkiye (AFAD) earthquake catalog, over 80,000 aftershocks occurred between February 6, 2023, and February 6, 2025. Eleven provinces were significantly affected and caused by severe damage and destruction.

Several active tectonic features, including segments of the EAFZ, the Malatya fault, and the Doğanşehir-Sürgü faults encircle the city of Malatya. Also, following the February 2023 Kahramanmaraş earthquakes, moderate to large aftershocks, as well as induced mainshocks, were observed to the NE of the EAFZ segments, specifically affecting the Pazarcık, Erkenek, and Pütürge areas, along with the Sürgü and Doğanşehir faults. The migration of aftershocks, particularly toward the NE, necessitates a thorough evaluation of the seismicity and earthquake hazard associated with Malatya. Notably, the Kale earthquake (M_W5.9) on October 16, 2024 (AFAD 2024c), occurred along an unnamed fault in Malatya that has been identified as a potential Quaternary tectonic feature by Emre et al. (2018). Akgün (2024) defined the unnamed fault as the Kale-Yeşilyurt Fault Zone.

The 6 February 2023 earthquake sequence significantly impacted an extensive region, driven not only by the substantial magnitudes of earthquakes but also by the complex slip distributions observed (Melgar et al. 2023). Surface ruptures measured approximately 300 km for the Pazarcık earthquake and around 150 km for the Elbistan earthquake, with peak slip values exceeding 8 m during the sequence (Jia et al. 2023; Alkan et al. 2024). The Pazarcık and Ekinözü earthquake doublets resulted in a cascading rupture across multiple segments of the southwestern section of the EAFZ, with significantly variable displacements. The post-seismic activities developed positive stress accumulation and deformation in the region, including the northeastern and southwestern parts of the EAFZ, Kale-Yeşilyurt, and Göksün segment, and the Malatya fault. These regions remained at hazard of strong earthquakes in the future (Akgün 2024; Liang et al. 2025). Also, a high number of aftershocks occur on the rupture zones along with the SW-NW Savrun fault, northeast between the Malatya fault and EAFZ, and northeast of Elazığ due to the positive stress change (Tan 2024). In the NE of the EAFZ, the Pütürge segment remained relatively stable, and significant stress accumulation was detected due to the dominant transtensional tectonic regime (Akgün et al. 2025). These factors have contributed to the changes in regional seismicity, with Malatya notably positioned at the northeastern termination of the 6 February 2023 sequence, an area with a high probability of stress transfer, thereby increasing its susceptibility to these seismic changes.

This study aims to analyze the Kale earthquake by examining not only the seismicity of the region and the tectonic activities surrounding Malatya from historical to contemporary times but also the 6 February 2023 earthquake sequence and its subsequent implications for Malatya and its environment. Numerous studies have been conducted on the regional and temporal evaluation of earthquake potential and seismic hazards in active zones both in Türkiye and globally (King et al. 1994; Console et al. 2000; Wan and Shen 2010; Öztürk 2020; Ormeni et al. 2023; Öztürk and Alkan 2023; Alkan et al. 2023; Yang et al. 2024). These assessments employ a variety of methodologies, including scaling laws, physical models, and various geophysical variables. Consequently, if the seismic and tectonic models of earthquake behavior can be grounded in a statistical framework, these approaches will significantly enhance the ability to estimate the likelihood of future earthquakes (Rundle et al. 2002). This integration of statistical analysis with seismic and tectonic data holds the potential to improve predictive capabilities and inform risk mitigation strategies. There are two primary approaches to studying earthquake potential. Firstly, the evaluation of experimental data based on earthquake indicators, often referred to as precursors. Secondly, the statistical analysis of earthquake behaviors (Holliday et al. 2007). The proposed paper employs statistical analyses to achieve its objective. Among the most fundamental and frequently utilized scaling tools in earthquake statistics are the *b*-value, the standard normal deviate *Z*-value (which indicates precursory seismic quiescence), the *Mc*-value (representing the cut-off or completeness magnitude), and the *Dc*-value (which describes the fractal dimension) (Öztürk and Alkan 2023). These metrics are instrumental in assessing the occurrence probability and return period of earthquakes. Additionally, time series analyses of seismic events and stress distributions are commonly employed to enhance the understanding of earthquake patterns and behaviors. Collectively, these tools contribute to a more robust statistical framework for evaluating seismic hazards.

This paper seeks to deepen the understanding of the tectonic settings that significantly contributed to the occurrence of the October 16, 2024, Kale earthquake. The analysis includes analyzing the *b*-value distributions, derived from the Gutenberg-Richter (G-R) relationship using a dataset of 14,549 earthquakes between 1905 and first half of 2024 within two adjacent zones in the study region. Also, the Coulomb stress variations associated with the aftershocks of the 6 February 2023 earthquake sequence and the Kale earthquake are imaged for various depths in a range from 0 to 20 km.

Tectonic structure in the region

The study area is predominantly influenced by several fault and fault zones, including Pütürge (PUS), Erkenek (ES), and Pazarcık (PAS) segments of the EAFZ, Çardak fault (CF), the Malatya fault (MF), Doğanşehir fault zone (DFZ), and Sürgü fault (SF) (Fig. 1). Additionally, it is partially affected by the Gerger (GS) and Narince (NS) segments of the Southeast Anatolia Thrust Zone (SEATZ). The MF is a 165-km-long left-lateral strike-slip fault that extends in an NE-SW direction. It is characterized by complex tectonic dynamics, as it branches into several segments. Notably, the southern segment, referred to as the Akçadağ segment (AS) (Emre et al. 2018), holds particular significance for the study region. The SF is an active left-lateral strike-slip fault segment within the EAFZ, extending approximately 70 km east–west. This fault traverses several settlements, including Çelikhan and Nurhak province (Balkaya et al. 2023). Although the instrumental earthquake history of this segment is relatively limited, the recent earthquake sequence and subsequent aftershocks on 6 February 2023 have drawn attention to its seismic significance with the Çardak fault. During the February earthquake sequence, the DFZ was primarily responsible for generating left-lateral aftershocks (Köküm 2024). Notably, the earthquake sequence of 1986 holds significant relevance for this fault. Following the 2023 earthquakes, a total rupture length of 30 km along the DFZ was documented by Softa et al. (2024). The PUS is situated between the southwestern margin of Lake Hazar and the Yarpuzlu district (Sincik, Adıyaman). This segment predominantly influences the formation of linear stream valleys within a mountainous landscape. Characterized by left-lateral strike-slip faulting, the Pütürge segment of the EAFZ has displayed notable surface deformations resulting from the 24 January 2020 Sivrice earthquake (Tatar et al.

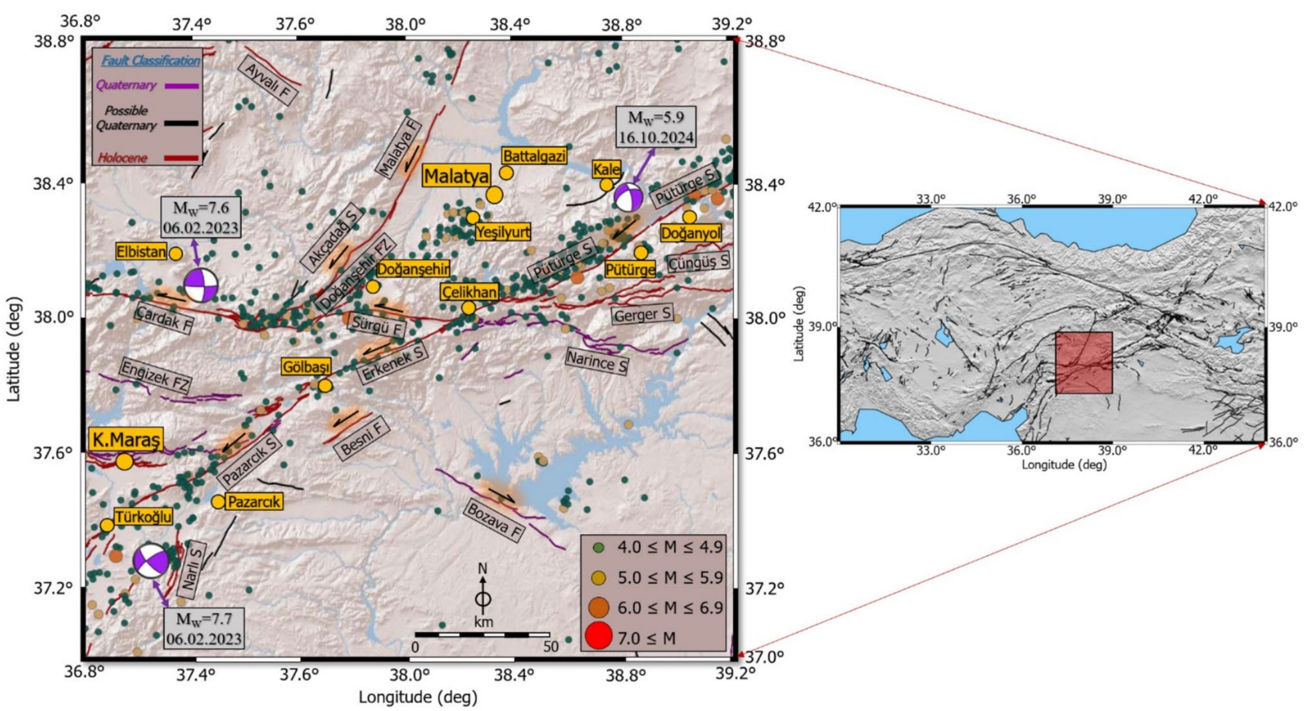

Fig. 1 Major tectonic elements of the study region. Claret red, purple, and black lines show the locations of Holocene, Quaternary, and Possible Quaternary faults taken from Emre et al. (2018). The names of faults and segments are obtained from Emre et al. (2018). Yellow circles represent provinces. Also, epicenter distributions of all earthquakes with $M_W \geq 4.0$ for the instrumental time. The magnitude distribution of earthquakes is represented with different symbols and catalog information and focal mechanism solutions of Kahramanmaras earthquake doublet and Kale earthquake were taken from the AFAD (https://deprem.afad.gov.tr/event-instrumental). On the right map, the red rectangle area indicates the study region. F: fault, S: segment, FZ: fault zone

2020). The Erkenek (ES) and Pazarcık (PAS) segments of the EAFZ are characterized as left-lateral strike-slip faults. These segments experienced significant displacement during the February 2023 earthquakes, notably during the event that occurred at 01:17 (UTC), $M_W = 7.7$. The surface ruptures were clearly seen on these segments and many roads and tunnels have been partly or completely demolished (Gokceoglu and Karahan 2023). The Gerger and Narince segments delineate the western boundary of the SEATZ and serve as an intersection point with the EAFZ. Both segments are classified as Holocene reverse faults (Emre et al. 2018).

Data for algorithms

For the *b*-value analysis, a homogeneous earthquake database according to moment magnitude (M_W) was compiled from (Tan 2021) for the time interval from 1905 to 2019. Tan (2021) proposed a homogeneous catalog and the equivalence M_W was the most suitable magnitude type for the earthquake hazard analysis. There were 377,429 events in this catalog for Türkiye and its vicinity between 1905 and 2019. In addition to this earthquake database, the events with local magnitude, M_L, between 2019 and first half of 2024 were compiled from the Kandilli Observatory and Earthquake Research Institute (KOERI 2023). There were 153,990 earthquakes around Türkiye at this time. To obtain a homogeneous database according to M_W between 2019 and first half of 2024, the empirical relationship from Tan (2021) for M_W-M_L conversion ($M_W = 1.017 \times M_L - 0.012$) was considered. Thus, 531,419 earthquakes occurred in Türkiye and its surroundings between 1905 and first half of 2024. After this step, the earthquakes were selected in the study area between 37.6°N-38.7°N and 37.4°E-39.2°E. Thus, 14,549 earthquakes with $1.0 \le M_W \le 6.9$ between December 4, 1905, and June 30, 2024, about 118.5 years. Then, the study area was divided into two sub-regions in order to compare the seismic hazard in details. Erdik et al. (1999) stated that seismic source zones are frequently determined using two fundamental tools: the seismicity profile and the tectonic structure of the region. Thus, the epicenter locations of whole events and the large main shocks with $M_W \ge 5.0$ for each region were plotted in Fig. 2 by taking into consideration the existing tectonic structure and the epicenter distributions of earthquakes with different magnitudes.

In addition to this earthquake database, 21 earthquakes ($M_W \ge 5.0$) that occurred in the study region after 6 February 2023 were used to investigate the Coulomb stress change. The focal parameters of earthquakes (dip, strike, rake, etc.) were taken from the Disaster and Emergency Management Authority (AFAD) shown in Table 1. Also, Fig. 3 demonstrates the focal mechanism solutions with epicenter locations, exhibiting strike-slip fault mechanisms. Considering the focal parameters of all events given in Table 1, event 1 represents the October 16, 2024 Kale earthquake. Within the scope of the study, the Coulomb stress change maps were created separately for 21 earthquakes and the October 16, 2024, Kale earthquake.

Methods

Gutenberg-Richter (G-R) magnitude-frequency relation

The magnitude-frequency distribution of earthquake occurrences can be described by an empirical relationship as seen in Eq. (1) proposed by Gutenberg and Richter (1944). This scaling law is one of the most widely utilized models in earthquake statistics, effectively illustrating the inverse relationship between the magnitude of an earthquake and its frequency of occurrence, and can be given as follows:

$$log_{10}N(M) = a - bM. \tag{1}$$

Here, *N(M)* represents the cumulative number of earthquakes occurring within a specified time interval with magnitudes equal to or greater than *M*. Notable variations can be observed in the *a*- and *b*-values, both of which are considered positive constants. The *a*-value is associated with the rate of seismic activity, while the *b*-value is derived from the slope of the frequency-magnitude relationship. This distinction underscores the importance of these parameters in characterizing the seismic behavior of a region. In various seismic regions, several factors influence variations in the *a*-value, including the spatial dimension of the study area, the time interval covered by the earthquake catalog, and the total number of recorded earthquakes. Conversely, the *b*-value is affected by a broader range of factors, such as anisotropic structural characteristics, tectonic features, stress distributions, geological complexity, thermal gradients, fault length, material properties, crack density, seismic attenuation, variations in seismic wave velocity, slip distribution, and strain conditions (Mogi 1962; Schorlemmer et al. 2005; Scholz 2015). Moreover, the relative distribution of small and large seismic events plays a significant role in influencing variations in the *b*-value. While the *b*-value can range from 0.3 to 2.0 on a global scale (Utsu 1971), it has been proposed that the average *b*-value approximates 1.0 (Frohlich and Davis 1993). Consequently, the *b*-value is recognized as a critical parameter for earthquake statistics in regions characterized by significant seismic and tectonic activity. Its importance lies in its ability to provide insights into the underlying processes governing earthquake occurrence and magnitude distribution. On the other hand, these multifaceted influences highlight the complexity which is

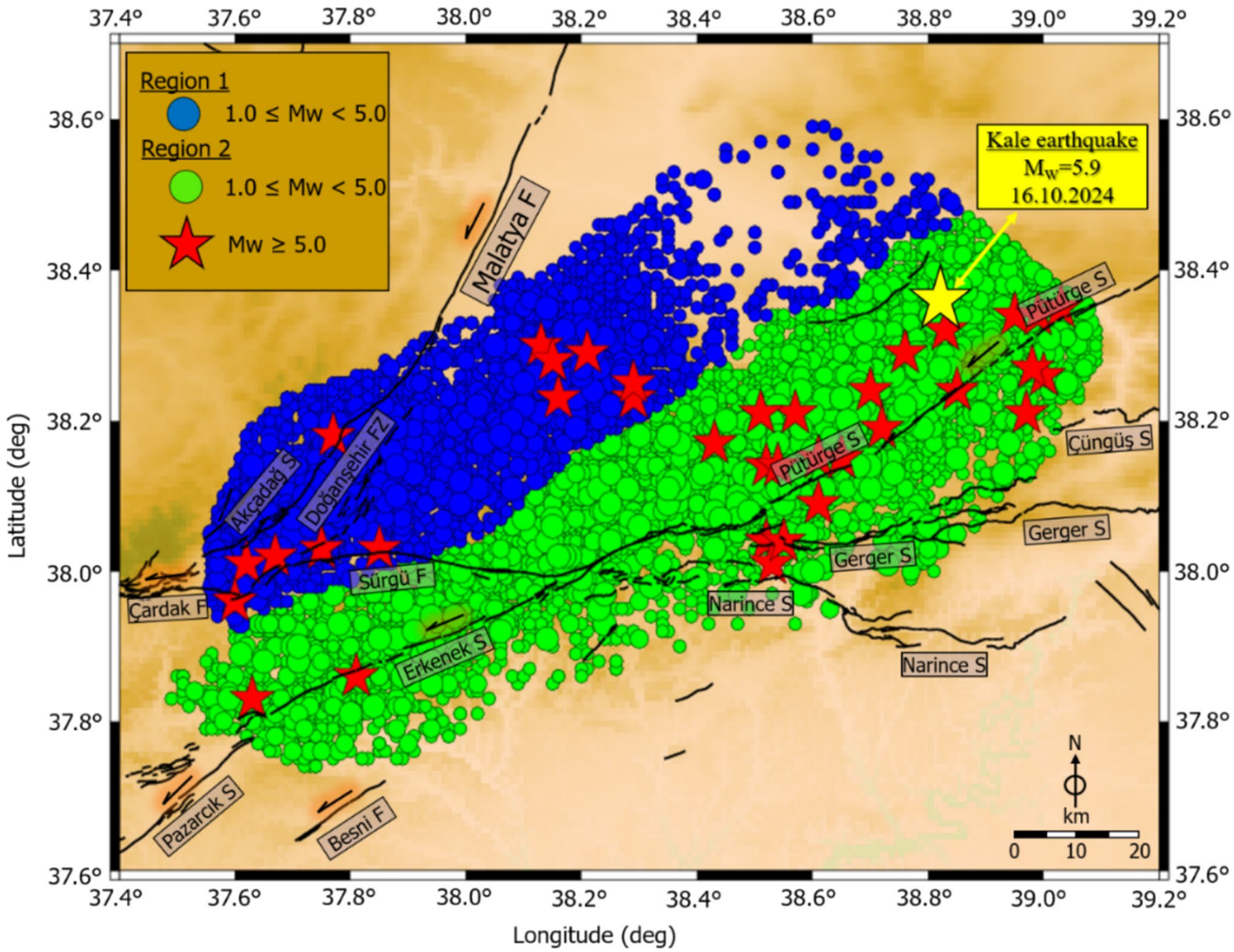

Fig. 2 Epicenter locations of 14,549 earthquakes with $M_W \geq 1.0$ from 1905 to 2024 for the study region. The seismicity catalog is taken from the KOERI website (https://udim.koeri.boun.edu.tr/). Magnitude levels of the events are plotted with different symbols. Region-1 and Region-2 are used to calculate for independent *b*-value distribution. Fault lines (thick black lines) and their names were taken from Emre et al. (2018)

involved in seismic analyses and hence, they emphasize the need for comprehensive assessments in the interpretation of seismic data.

In numerous studies related to changes in seismicity rates, particularly in the calculation of the *b*-value, it is essential to utilize the maximum number of recorded earthquakes to ensure reliable and high-quality results. In this context, the estimation of magnitude completeness, referred to as the *Mc*-value, which represents the minimum magnitude at which a complete recording of seismic events occurs, must be the initial step before conducting such analyses. This process is critical, as it establishes a foundation for accurate assessments of seismic activity and enhances the integrity of the subsequent statistical evaluations. The *Mc*-value is determined from the magnitude-frequency distribution of earthquakes, representing the completeness level that includes approximately 90% of seismic events (Wiemer and Wyss 2000). It is well known that the *Mc*-value has a decreasing trend in time related to the number of seismographs increases in the regions. It is also important to note that the *Mc*-value may be higher during the early part of the earthquake catalog due to the lack of networks. Therefore, as smaller events may remain undetected or unlocated, often falling within the coda of larger earthquakes (Wiemer and Katsumata 1999). If great *Mc*-values are not included in the catalog, the minimum magnitude threshold can be reduced and number of the earthquakes to be used in the calculations can be increased. For the seismic hazard assessments which use the complete sets of small earthquakes, the minimum magnitude level must be increased to the largest *Mc*-value (Wiemer and Wyss 2000). The *Mc*-value varies regionally, influenced by the seismic activity of the area under investigation and the detectability of the seismic

Table 1 Focal mechanism parameters of selected earthquakes taken from the AFAD (https://tdvms.afad.gov.tr/) website

No	Date	Latitude (°N)	Longitude (°E)	Depth (km)	Magnitude	Strike (°)	Dip (°)	Rake (°)	Fault type
1	2024–10-16 T07:46:31	38.365	38.808	10.48	5.9	348	71	− 140	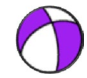
2	2024–01-25 T13:04:04	38.198	38.458	13.88	5.2	177	72	− 164	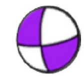
3	2023–11-23 T14:46:08	38.158	38.569	7.00	5.2	146	73	− 169	
4	2023–08-24 T05:35:23	38.309	38.171	7.00	5.0	351	81	− 150	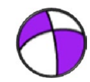
5	2023–08-10 T17:48:00	38.308	38.209	7.90	5.3	230	50	− 18	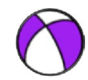
6	2023–02-27 T09:04:49	38.272	38.303	6.15	5.6	353	62	163	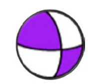
7	2023–02-10 T04:50:23	38.235	38.141	10.45	5.0	247	81	1	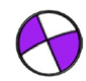
8	2023–02-08 T11:11:51	38.012	37.641	13.18	5.3	300	62	20	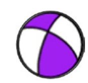
9	2023–02-07 T10:18:11	38.125	38.561	6.85	5.1	249	83	− 14	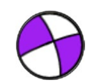
10	2023–02-07 T07:11:13	38.159	38.632	8.18	5.3	54	82	24	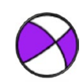
11	2023–02-07 T03:08:55	37.975	37.629	6.87	5.0	8	69	142	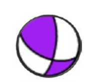
12	2023–02-07 T03:13:12	37.808	37.655	8.44	5.4	224	83	− 173	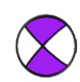
13	2023–02-06 T20:40:05	38.240	38.070	5.82	5.2	162	45	− 172	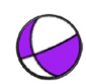
14	2023–02-06 T15:33:31	38.239	38.182	11.15	5.3	244	70	13	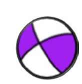
15	2023–02-06 T15:14:32	37.977	37.667	7.04	5.0	30	74	170	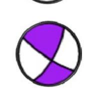
16	2023–02-06 T13:39:23	38.037	37.628	7.20	5.3	316	87	145	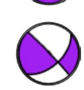
17	2023–02-06 T10:51:30	38.305	38.151	10.4	5.7	241	33	107	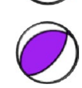
18	2023–02-06 T10:35:57	38.172	37.920	11.28	5.9	31	31	32	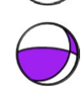
19	2023–02-06 T02:06:22	38.084	38.368	6.95	5.1	93	38	− 73	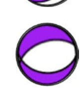

Table 1 (continued)

No	Date	Latitude (°N)	Longitude (°E)	Depth (km)	Magnitude	Strike (°)	Dip (°)	Rake (°)	Fault type
20	2023–02-06 T02:03:35	37.898	37.957	10.23	5.6	241	56	31	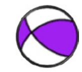
21	2023–02-06 T01:30:28	38.117	38.509	7.00	5.0	328	51	− 171	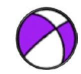

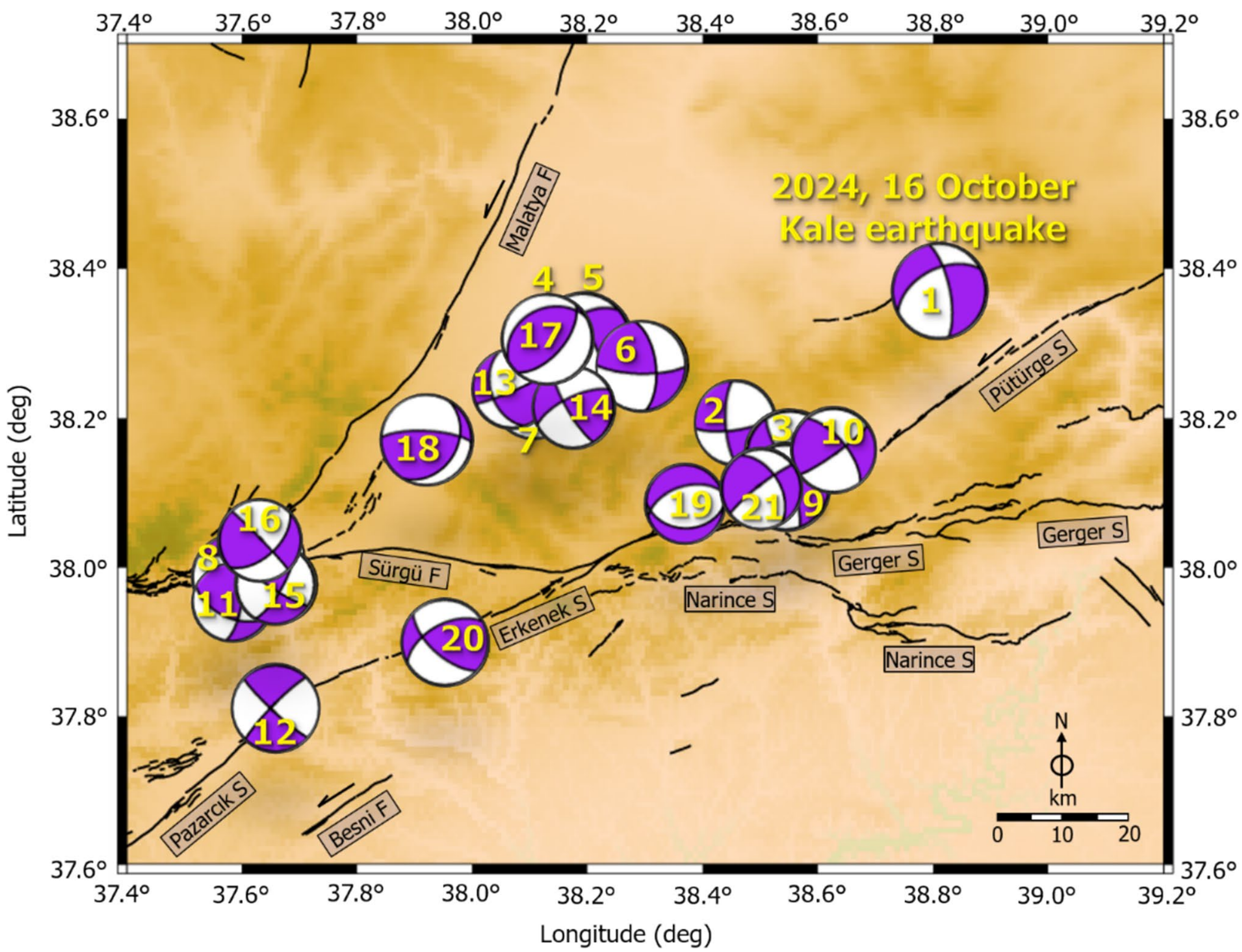

Fig. 3 The earthquake ($M_W \geq 5.0$) fault mechanism solutions for the study area**.** Purple beach balls represent the solutions. The parameters of the focal mechanism solution are given in Table 1. Fault lines (thick black lines) and their names were taken from Emre et al. (2018)

network. These temporal variations in the *Mc*-value can significantly impact statistical results. Therefore, it is essential to monitor changes in the *Mc*-value with precision. Employing a moving time window approach in conjunction with the maximum likelihood method may enhance the accuracy of these assessments (Wiemer and Wyss 2000).

Variations in Coulomb stress

Earthquakes, as natural phenomena, result from the release of stress when shear forces acting along fault planes exceed the fault's strength (Yang et al. 2024). As such, changes in Coulomb stress are critical for analyzing the stress variations induced by seismic events (Peikert et al. 2023).

Consequently, Coulomb stress analysis is a well-established method for investigating stress changes that may lead to failure in the source fault. This analytical approach plays a vital role in understanding the mechanisms underlying earthquake initiation and propagation, facilitating improved risk assessment and mitigation strategies.

The variation in Coulomb failure stress ($\Delta\sigma_{cfs}$) on the receiver fault is determined by:

$$\Delta\sigma_{cfs} = \Delta\tau_s + \mu\prime\Delta\sigma_{n\prime}. \quad (2)$$

Here, $\Delta_{\tau s}$ represents the change in shear stress associated with the positive direction of slip on the receiver fault, while $\Delta\sigma_{n'}$ denotes the change in normal stress along the fault plane. The $\mu\prime$ indicates the effective friction coefficient on the fault (King et al. 1994; Lin and Stein 2004; Toda et al. 2011). This coefficient accounts for the effects of pore-pressure changes and can vary between 0 and 1. For this study, we adopt a value of 0.4 for the effective friction coefficient in an elastic half-space (Toda et al. 2005; Wan and Shen 2010). The dimensionless friction coefficient is chosen concerning the left-lateral strike-slip fault mechanism of the receiver fault (King et al. 1994; Njinju et al. 2025). Additionally, we assume a dimensionless Poisson's ratio (ν) of 0.25, while Young's modulus (E) is selected as 8×10^5 bars. Coulomb stress variations within the range of -0.1 to 0.1 bar are considered adequate for predicting subsequent earthquake hazards (Yadav et al. 2012). An increase in Coulomb stress changes signifies loading stress that promotes the likelihood of brittle failure along the fault, whereas a decrease in these changes may reflect unloading stress, which acts to inhibit the occurrence of an earthquake rupture (Stein et al. 1994; Liao et al. 2022; Peikert et al. 2023). Considering the elastic parameters, the static stress changes on the specified receiver faults of the study region were calculated by using the focal mechanism parameters (dip, strike, rake, depth, magnitude) of 20 earthquakes. The Coulomb stress change in the Kale earthquake was also mapped using its focal parameters given in Table 1, event no 1.

Results

This study presents a statistical assessment of seismic activity leading up to the Mw 5.9 Kale earthquake in Malatya, Türkiye, using various seismotectonic parameters, including the b-value from the Gutenberg-Richter relationship and changes in Coulomb stress. The *b*-value of the G-R relationship was estimated using the maximum likelihood method, which provides a more robust estimation compared to the least squares method (Aki 1965). Estimation of *Mc*-value is achieved by considering G-R power low distribution of magnitudes (Eq. 1). The spatial variation of the Mc-value was analyzed on a grid with a resolution of $0.01° \times 0.01°$ in both longitude and latitude for Regions 1 and 2, as shown in Fig. 4. The Mc-values range from 1.7 to 2.4 in Region 1 (Fig. 4a) and from 1.7 to 2.3 in Region 2 (Fig. 4b). In both regions, the Mc-values predominantly cluster within the range of 1.7 to 2.2. However, higher values of 2.3 and 2.4 are observed in relatively small localized areas, particularly in the southwestern part of Region 1, and only occasionally in Region 2. Furthermore, the magnitude–frequency distributions of earthquakes in Regions 1 and 2 are illustrated in Fig. 5. Based on these distributions, an Mc-value of 2.1 is considered appropriate for both regions, as it effectively represents both the spatial and overall seismic characteristics. Therefore, for Region-1, the *Mc*-value was taken as 2.1, and the *a*- and *b*-values were estimated at 5.04 and 0.78 ± 0.04, respectively (Fig. 5a). Additionally, the *Mc*-value for Region-2 was set at 2.1, with the *a*- and *b*-values calculated as 5.27 and 0.84 ± 0.07, respectively (Fig. 5b). The maximum likelihood method was used to calculate *a*- and *b*-values and their confidence limits (Aki 1965). The standard deviation of *b*-value (95% confidence limit) is calculated using the equation suggested by Aki (1965) as $\pm 1.96b/\sqrt{n}$, where n is the number of earthquakes used (many details can be found in Tinti and Gasperini (2024). As previously mentioned, the *b*-value typically ranges from 0.3 to 2.0 on a global scale, with tectonic events generally exhibiting *b*-values between 0.5 and 1.5. Given that the average *b*-value is proposed to be approximately 1.0, the observed *b*-values of 0.78 and 0.84 for the two regions can be considered relatively low. Furthermore, as illustrated in Fig. 5, the magnitude-frequency distribution of earthquakes in the two regions aligns closely with the G-R relationship.

Figure 6 illustrates the regional distributions of *b*-values for the first half of 2024. To visualize the *b*-value distribution, a moving window technique from the *ZMAP* software (Wiemer 2001) was employed, utilizing different sample sizes (1850 events for Region-1 and 1400 events for Region-2) and a regional grid of 0.01° by 0.01° for both longitude and latitude across each region. As suggested by Wiemer (2001), the radius is fixed by adjusting the number of earthquakes within each grid cell. The chosen grid size and sample event counts align with the accuracy of epicentral determinations in the catalog, ensuring continuous and dense spatial coverage. Fixed Mc-value and a constant number of events exceeding the Mc are used in both regions. Additionally, earthquakes are selected within circular/polygonal areas for each node in the b-value map. After testing various input values for image verification, it was found that these b-value areas are more visibly distinct on a regional scale, leading to more reliable results. The process and determined outputs are consistent with G–R relationship and their relative fits. Regional variations in *b*-values range from 0.6 to 1.1 across the two studied regions. As indicated by Frohlich and Davis

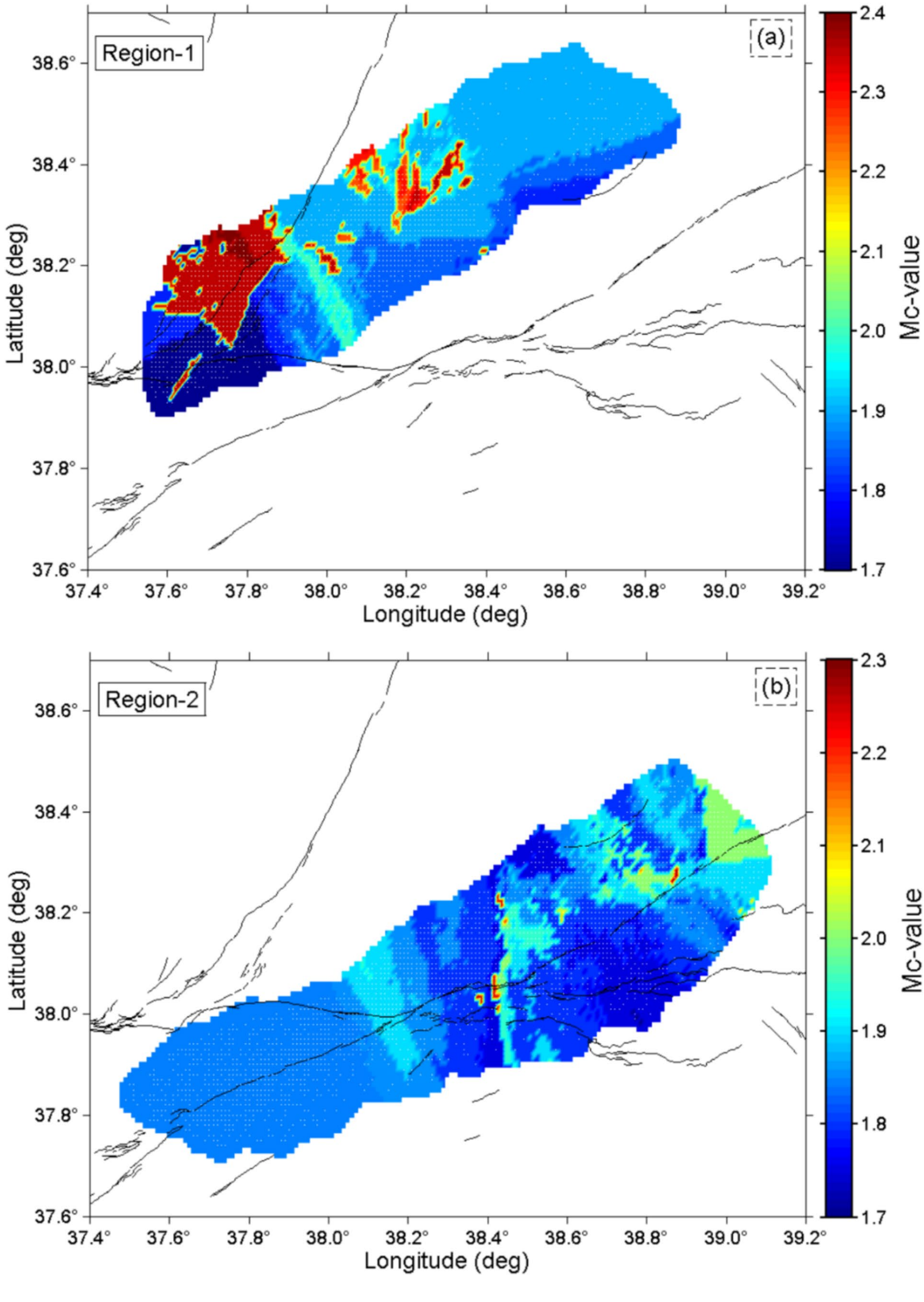

Fig. 4 Spatial variation of Mc-value in a grid of $0.01^\circ \times 0.01^\circ$ in longitude and latitude for **a** Region-1 and **b** Region-2

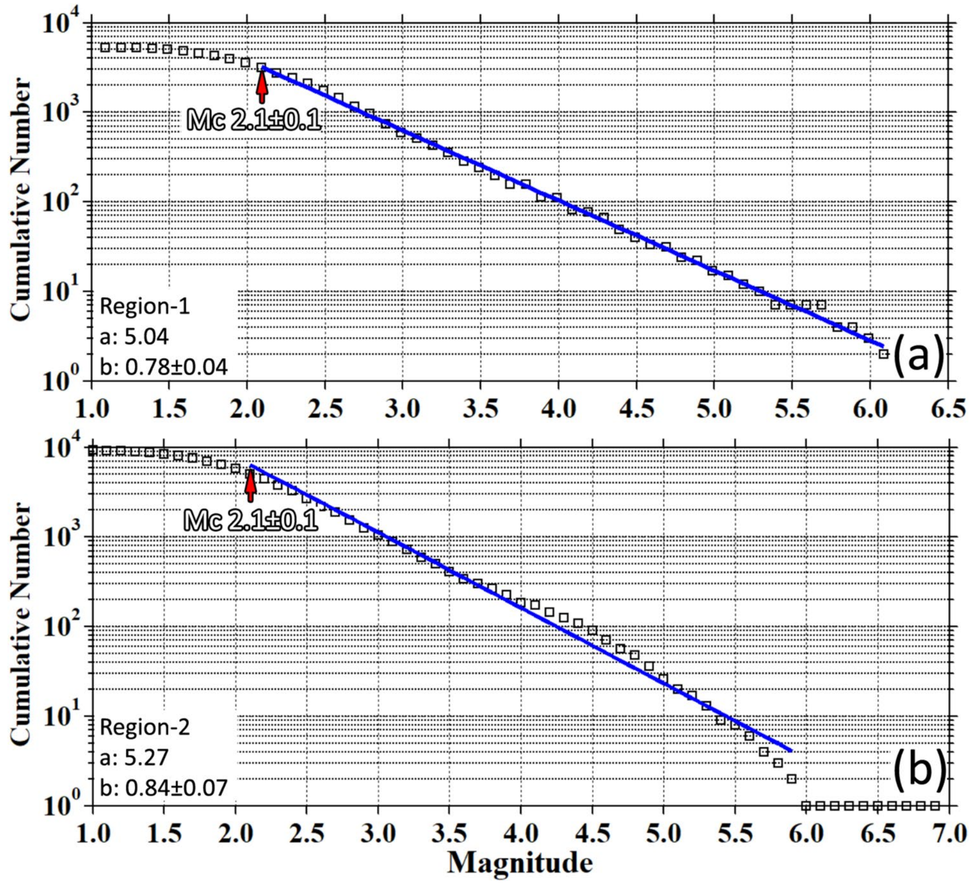

Fig. 5 Magnitude-frequency distribution of the earthquakes and *b*-value of *G-R* relation, **a** for Region-1 and **b** for Region-2. *b*-value, its standard deviation, *a*-value, and *Mc*-value are given in the figure

(1993), the *b*-value of the G-R relationship is typically represented by an average value of $b = 1.0$. Considering this average value, we can say that significant decreases in *b*-values (less than 0.7) were identified in Region-1. As illustrated in Fig. 6a, these areas particularly cover the Akçadağ Segment, Sürgü Fault, and Doğanşehir Fault zone. In the Kale-Malatya-Doğanşehir provinces, the *b*-value ranges from 0.8 to 0.9, while other regions exhibit *b*-values exceeding 1.0. Similarly, pronounced decreases were noted in Region-2 (Fig. 6b), encompassing the NS, GS, and PUS areas. Additionally, *b*-values between 0.8 and 0.9 were observed in the ES and SF segments, as well as in the Çelikhan, Doğanyol, and the western and southern portions of Kale. In contrast, the *b*-values greater than 1.0 were estimated in the eastern and northern parts of Kale. Regions exhibiting higher *b*-values typically correspond to a greater frequency of small-magnitude seismic events, while areas characterized by lower *b*-values are generally associated with the occurrence of larger-magnitude earthquakes (Fig. 2). Laboratory studies on rock fracture show that a decreasing trend is associated with a reduction in the confining pressure and an increase in the applied shear stress (Scholz 1968). It is suggested that large *b*-values are related to an increase in the thermal gradient, fracture density, or material heterogeneity in the geological complexity. Previous studies show that *b*-value is also related to the anisotropic environments, fault length, strain circumstances, seismic wave velocity changes and attenuation and slip distribution, etc. (Mogi 1962; Ogata et al. 1991; Schorlemmer et al. 2005; Ansari 2016). Consequently, the regional distribution of the *b*-values demonstrates a strong correlation with the underlying geological, seismic, tectonic and physical conditions of the structures.

Figures 7 and 8 present the results of Coulomb stress changes at depth ranges of 5, 10, 15, and 20 km, based on selected regional events, excluding the October 16, 2024, Kale earthquake. Additionally, Fig. 8 illustrates the Coulomb stress maps, along with vertical cross sections oriented in the NW–SE and NE-SW directions corresponding to the Kale earthquake. All selected earthquakes with magnitudes greater than or equal to $M_W \geq 5.0$ occurred following the main shocks of February 6, 2023, as outlined in Table 1. Coulomb stress-depth maps revealed that positive stress lobes (greater than 0.0 bars) emerged along the PUS, ES, and PAS segments of the EAFZ. Additionally, positive stress changes were noted in the N-NE direction along the SF and MF, although these changes exhibited a scattered distribution. Notably, in the direction of the Doğanşehir, Malatya, Kale, and Pütürge-Doğanyol provinces, positive stress values were observed to form an arc considering all depth intervals, merging from the EAFZ in the northeastern part of the study

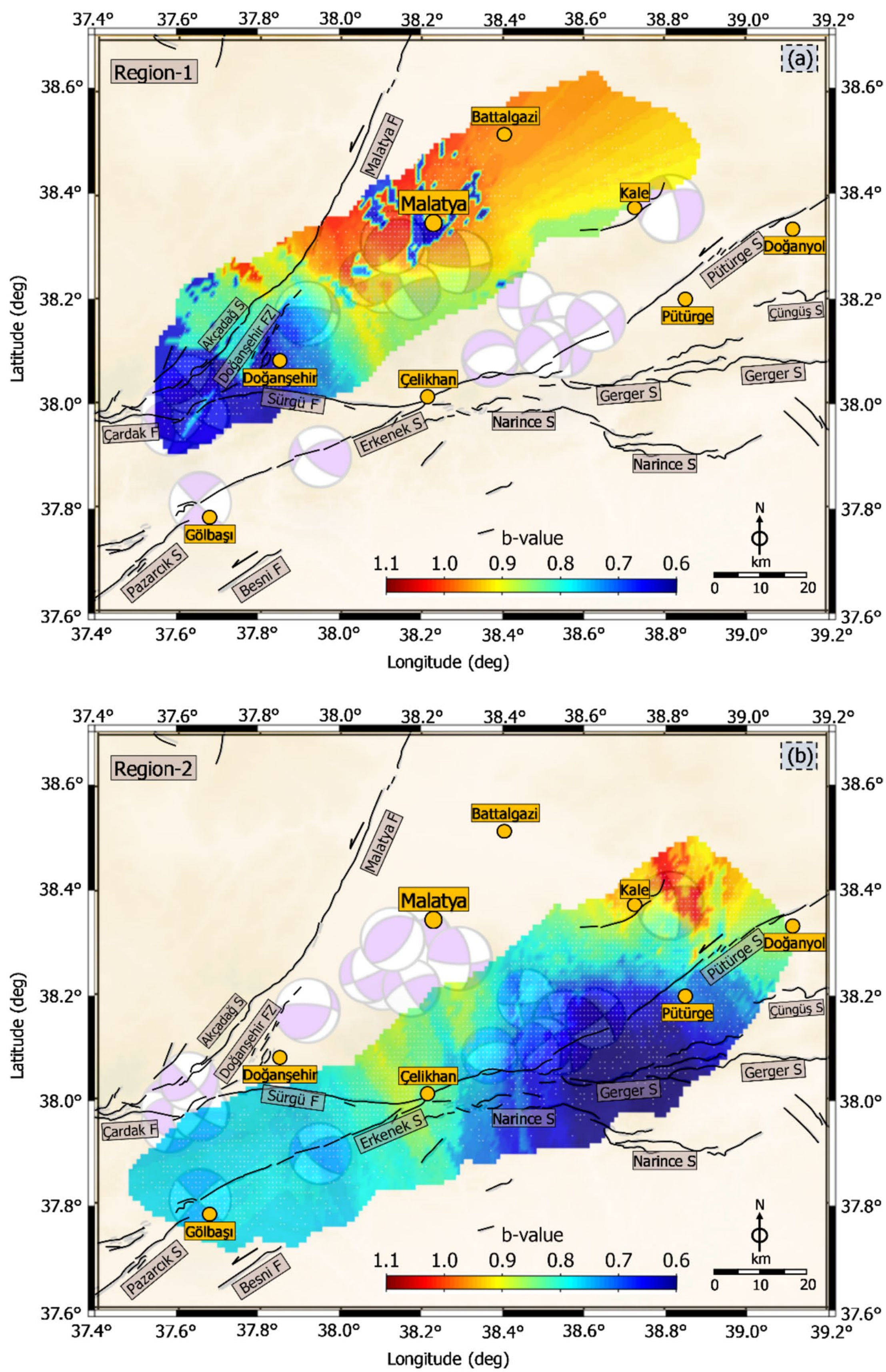

Fig. 6 Spatial variations of *b*-values **a** for Region-1 and **b** for Region-2

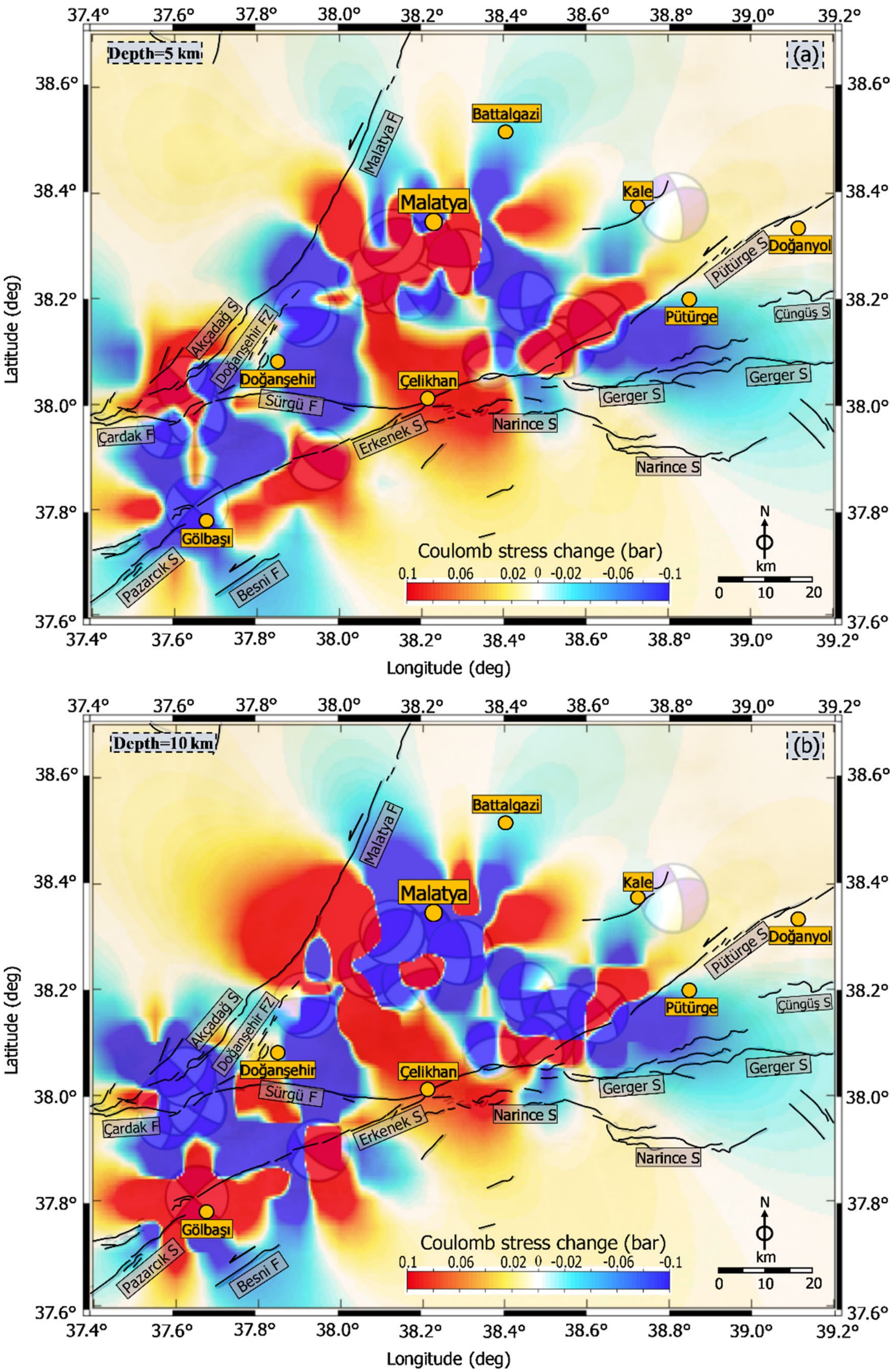

Depth=5 km
(a)
Battalgazi
Malatya F
Malatya
Kale
Doğanyol
Pütürge S
Pütürge
Çüngüş S
Akçadağ S
Doğanşehir FZ
Doğanşehir
Çelikhan
Sürgü F
Gerger S
Gerger S
Çardak F
Erkenek S
Narince S
Narince S
Gölbaşı
Pazarcık S
Besni F
Coulomb stress change (bar)
0.1 0.06 0.02 0 -0.02 -0.06 -0.1
N
km
0 10 20
Latitude (deg)
Longitude (deg)
37.4° 37.6° 37.8° 38.0° 38.2° 38.4° 38.6° 38.8° 39.0° 39.2°
37.6° 37.8° 38.0° 38.2° 38.4° 38.6°
Depth=10 km
(b)
Battalgazi
Malatya F
Malatya
Kale
Doğanyol
Pütürge S
Pütürge
Çüngüş S
Akçadağ S
Doğanşehir FZ
Doğanşehir
Çelikhan
Sürgü F
Gerger S
Gerger S
Çardak F
Erkenek S
Narince S
Narince S
Gölbaşı
Pazarcık S
Besni F
Coulomb stress change (bar)
0.1 0.06 0.02 0 -0.02 -0.06 -0.1
N
km
0 10 20
Latitude (deg)
Longitude (deg)

◂**Fig. 7** Coulomb stress change maps prepared from the earthquakes (transparent purple beach balls) are listed in Table 1 for the different depths: **a** 5 km and **b** 10 km. Black lines show the locations of active faults taken from Emre et al. (2018). The dark yellow circles represent province locations

region. On the other hand, despite the absence of any designated active fault in Malatya city center and its vicinity on the active fault map of Turkey (Emre et al. 2018), this region experienced a medium-sized earthquake ($M_W \geq 5.0$). This seismic event facilitated the transfer of positive stress values to the unnamed fault located near Kale and the PUS in the SE portion of the study area. The focal mechanism solutions depicted as transparent purple beach balls in Figs. 7 and 8 offer insights into the generation of positive stress values in the region. Conversely, while negative stress changes (less than 0.0 bars) were identified as small lobes at each depth level on the stress maps, these negative lobes were effectively countered by the presence of positive stress lobes across all depth levels. Negative stress values were observed along the northern segment of the MF. Additionally, negative stress changes were detected at depths ranging from 5 to 10 km in the vicinity of Doğanşehir and the south of the Pütürge. In the Coulomb stress distribution covering the first 5 km depth, linear stress effects are prominent in the Erkenek Segment, particularly in the area between Çelikhan and Pütürge to the northeast of Çelikhan and between Çelikhan and Gölbaşı to the southwest. These stress effects, likely caused by aftershocks, are observed to be limited at a depth of 10 km. However, a significant stress situation is particularly noticeable between Çelikhan and Malatya (Fig. 7). In the stress map at a depth of 10 km, the stress is concentrated along the Malatya Fault and the Sürgü Fault (Fig. 7). The stress situation at a depth of 15 km clearly shows that the stress along the Sürgü Fault is prominently highlighted and continues at a depth of 20 km (Fig. 8). On the other hand, the stress change maps at depths of 15 and 20 km indicate that the area between Malatya and Çelikhan is under significant stress (Fig. 8). In this case, it is expected that future seismic activity could occur along the EAF's Gölbaşı direction, the Sürgü Fault, the southwest of Pütürge, and the Malatya Fault. The Coulomb stress change map associated with October 16, 2024, Kale earthquake ($M_W = 5.9$) and vertical cross sections are presented in Fig. 8. The cross sections provide a detailed representation of the northwest-southeast (NW–SE) oriented negative stress lobes and the northeast-southwest (NE-SW) oriented positive stress lobes at a depth of 20 km. Furthermore, the cross sections include the distribution of aftershocks (indicated by orange dots) that occurred between October 16 and October 25, 2024. Before the Kale earthquake, analyses of local seismicity and stress change maps indicated positive stress transfer, particularly toward the E and NE around Malatya, aligned with the EAFZ. Notably, no seismic activity was observed between the provinces of Malatya and Kale (Figs. 7 and 8). The positive stresses illustrated in Fig. 9 were predominantly transferred in a NW–SE orientation. In the A-B cross section (Fig. 9a), clusters of aftershocks were observed beneath the epicentral region of the main shock ($M_W = 5.9$ Kale earthquake) and around the hypocentral area; however, aftershocks were notably absent in the SE and NW directions. In contrast, the aftershock distribution shown in the C-D cross section primarily extended in the NE rather than the SW direction (Fig. 9b). This pattern of aftershock activity may provide insights into future local seismicity along the NE oriented structures parallel to the EAFZ.

Discussions

The earthquake sequence of February 6, 2023, along with its aftershocks, was distributed over a broad region and had a significant impact on the tectonic regime, particularly affecting the various segments of EAFZ. Notably, a large portion of aftershocks outside the immediate vicinity of the main shocks were concentrated around Malatya. The occurrence of the October 16, 2024, Kale earthquake further underscores the need for a comprehensive reassessment of seismic activity in the Malatya region. The proposed paper aims to elucidate not only the tectonic factors contributing to the Kale earthquake but also to identify potential faults in and around Malatya through the analysis of the *b*-values derived from the G-R relationship and the assessment of Coulomb stress changes. The analyses are grounded in several key components: first, the observation of Coulomb stress changes resulting from earthquakes of magnitude $M_W \geq 5.0$ that occurred after February 2023; second, the evaluation of *b*-value variations utilizing homogeneous earthquake catalogs from the instrumental period; and third, the examination of the distribution and clustering of aftershocks recorded during the instrumental period within the study region. This multifaceted approach aims to enhance the understanding of seismic risks and tectonic behavior in the region, contributing to improved earthquake preparedness and risk mitigation strategies.

It is well established that low *b*-values are indicative of regions under high stress (Scholz 2015; Öztürk and Alkan 2023; Alkan et al. 2023). Akar (2024) demonstrated that very low *b*-values were associated with the Pazarcık earthquake, while relatively lower *b*-values were noted in the vicinity of the Elbistan earthquake. Furthermore, the significant temporal reductions in *b*-values occurred before the mainshock events (Öztürk and Şahin 2019). Also, Sharma and Biswas (2025) reported that *b*-values ranged from 0.7 to 1.1 in the region affected by the February 2023 earthquakes, highlighting that these seismic events

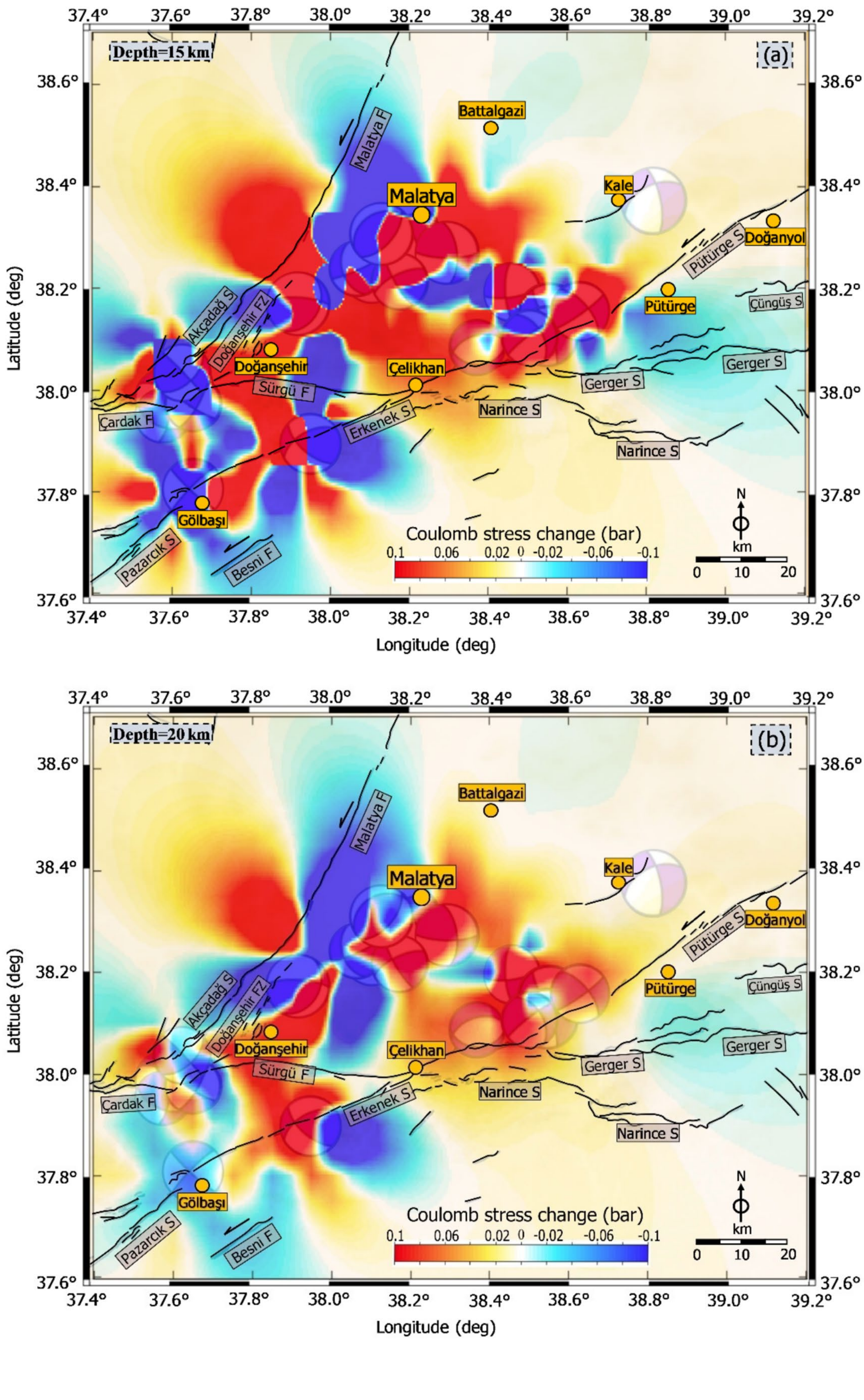
Depth=15 km
(a)
Depth=20 km
(b)
Malatya F
Battalgazi
Kale
Malatya
Doğanyol
Pütürge S
Pütürge
Çüngüş S
Akçadağ S
Doğanşehir FZ
Doğanşehir
Sürgü F
Çelikhan
Gerger S
Çardak F
Erkenek S
Narince S
Gölbaşı
Pazarcık S
Besni F
Coulomb stress change (bar)
0.1 0.06 0.02 0 -0.02 -0.06 -0.1
N
km
0 10 20
Latitude (deg)
Longitude (deg)
37.4° 37.6° 37.8° 38.0° 38.2° 38.4° 38.6° 38.8° 39.0° 39.2°
37.6° 37.8° 38.0° 38.2° 38.4° 38.6°

◂**Fig. 8** Coulomb stress change maps prepared from the earthquakes (transparent purple beach balls) are listed in Table 1 for the different depths: **a** 15 km and **b** 20 km. Black lines show the locations of active faults taken from Emre et al. (2018). The dark yellow circles represent province locations

primarily occurred in areas with low *b*-values (below 1.0). This study suggests that variations in *b*-values, both preceding and following mainshocks, correlate with stress changes in the region. Specifically, low *b*-values are associated with positive stress distributions in the possible earthquakes. The analysis of *b*-value variations indicates that consistently low values (ranging from 0.6 to 1.1) are observed in both Region-1 and Region-2 (Fig. 6). These findings suggest that the study region is under positive stress loading. Notably, the Akçadağ segment, which encompasses the western part of the study area, along with the Sürgü fault and the Doğanşehir fault zone, exhibits

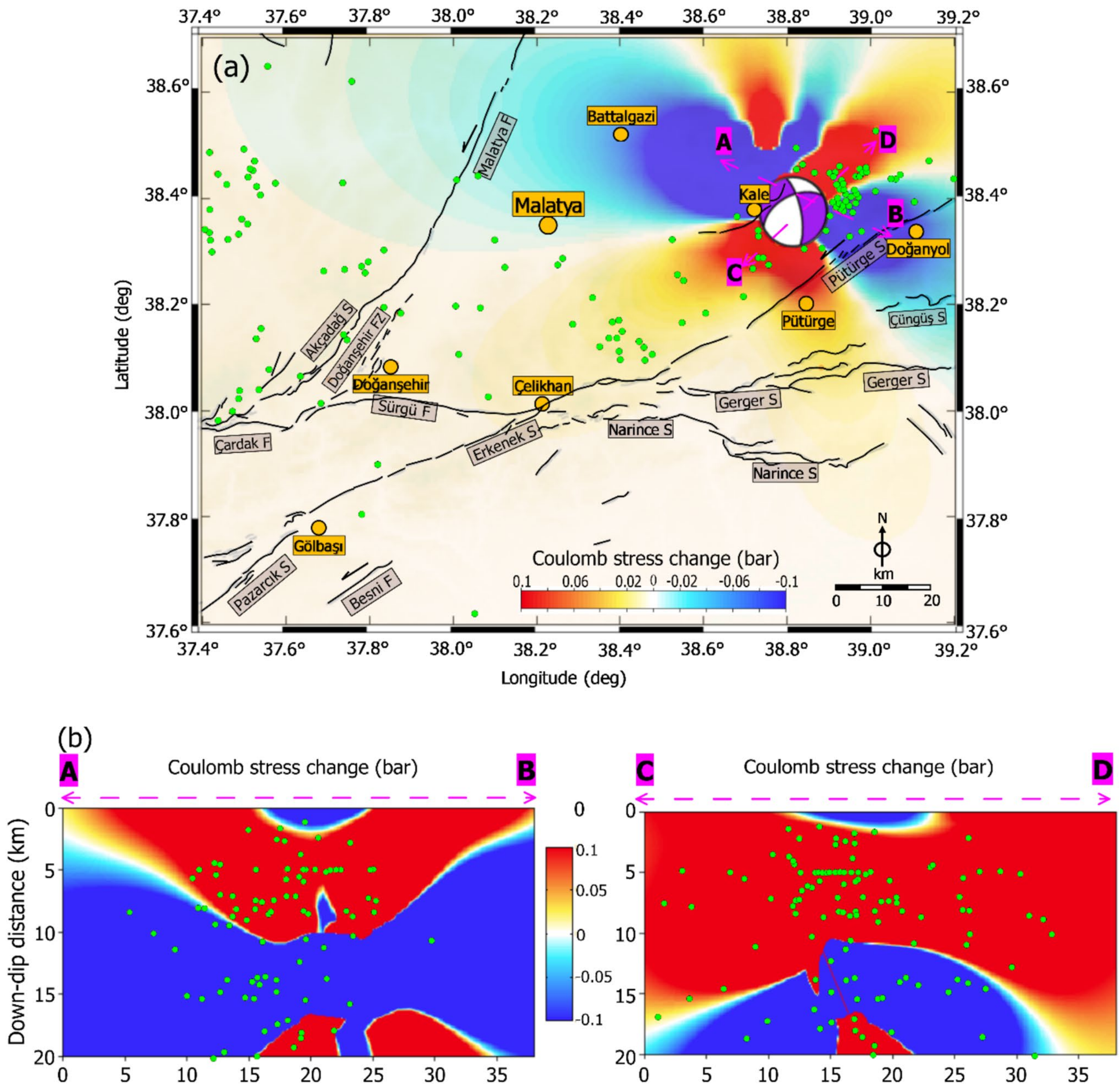

Fig. 9 **a** The coulomb stress change map for 2024, 16 October M_W 5.9 Kale earthquake (transparent purple beach ball) is shown in Table 1 for the hypocenter depth. Black lines show the locations of active faults taken from Emre et al. (2018). The dark-yellow circles represent province locations **b** The NW–SE and NE- SW-oriented vertical cross sections along with the profiles A–B and C–D within the depth range of 0–20 km, respectively. Orange dots depict the seismic activity in the region in time between 16 October 2024 and 25 October 2024, obtained from the KOERI earthquake catalog (http://www.koeri.boun.edu.tr/sismo/zeqdb/)

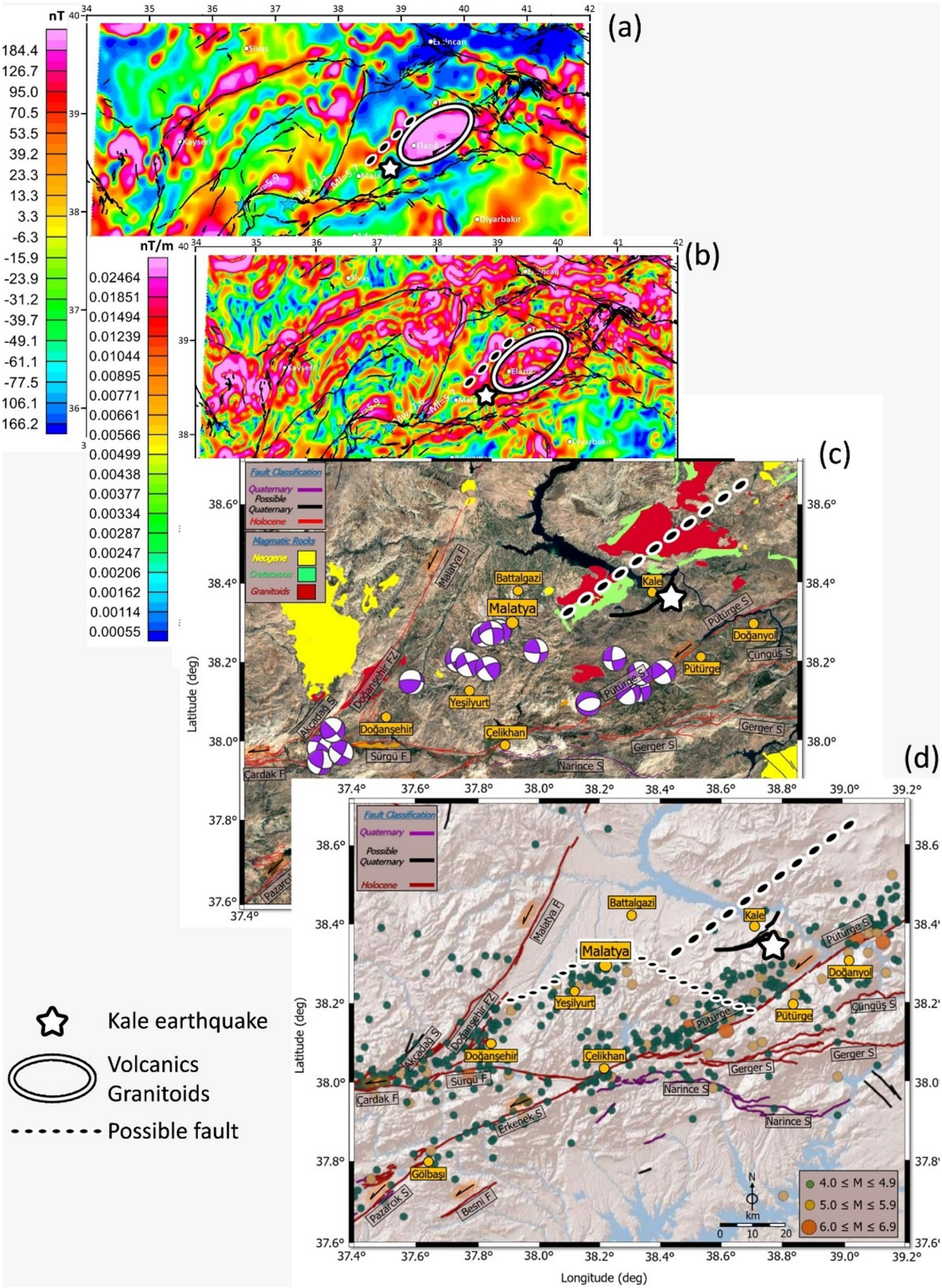
(a)
nT
184.4
126.7
95.0
70.5
53.5
39.2
23.3
13.3
3.3
-6.3
-15.9
-23.9
-31.2
-39.7
-49.1
-61.1
-77.5
106.1
166.2
Sivas
Erzincan
Kayseri
Elazığ
Diyarbakır
(b)
nT/m
0.02464
0.01851
0.01494
0.01239
0.01044
0.00895
0.00771
0.00661
0.00566
0.00499
0.00438
0.00377
0.00334
0.00287
0.00247
0.00206
0.00162
0.00114
0.00055
(c)
Fault Classification
Quaternary
Possible Quaternary
Holocene
Magmatic Rocks
Neogene
Cretaceous
Granitoids
Battalgazi
Malatya
Kale
Pütürge S
Doğanyol
Çüngüş S
Pütürge
Yeşilyurt
Doğanşehir
Doğanşehir FZ
Akçadağ S
Malatya F
Çelikhan
Gerger S
Sürgü F
Narince S
Çardak F
Latitude (deg)
(d)
Kale earthquake
Volcanics
Granitoids
Possible fault
Erkenek S
Gölbaşı
Pazarcık S
Besni F
4.0 ≤ M ≤ 4.9
5.0 ≤ M ≤ 5.9
6.0 ≤ M ≤ 6.9
km
0 10 20
Longitude (deg)

◂**Fig. 10** **a** Reduction to the pole of the magnetic anomalies and **b** Application of total horizontal derivative, taken from Büyüksaraç et al. (2024). **c** The magmatic rocks and active faults (taken from Akbaş et al. (2011) and Emre et al., (2018), and focal mechanism solutions of the earthquakes ($M_W \geq 5.0$) occurring after 6 February 2023 (taken from AFAD earthquake catalog (https://tdvms.afad.gov.tr/)). **d** Potential fault oriented toward the city center of Malatya (dashed line) and other major tectonic elements in the study region

particularly low *b*-values (Fig. 6a). Correspondingly, positive Coulomb stress variations are observed around this intersection of fault lines, indicating that positive stress transfer is ongoing along the Doğanşehir fault zone in the N-NE direction relative to the Malatya fault, at 15 km depth particularly (Fig. 7a).

Dai et al. (2024) reported that the rupture length of the Pazarcık earthquake was approximately 360 km, while the Elbistan earthquake had a rupture length of about 220 km. These events were associated with stress transfer that impacted the Çardak fault and the Doğanşehir fault zone. Zhao et al. (2023) calculated the peak slip values for the Pazarcık and Elbistan earthquakes at 9.7 m and 10.8 m, respectively. The coseismic stress disturbances resulting from these significant earthquakes led to substantial stress accumulation in adjacent active fault regions, thereby heightening the rupture risk along both the Malatya fault and the northeastern Pütürge segment in a depth range of 15and 20 km (Fig. 8). This finding is supported by the most recent earthquake that occurred south of Kale (Malatya) on February 17, 2025, at 18:41, with MW 4.5 (AFAD 2025). Li et al. (2023) focused on the stress transfer mechanisms associated with the February 2023 earthquakes, concluding that the static stress transfers from the EAFZ to the Sürgü fault occurred through the unclamping of the fault interface. Significant positive stress values were estimated in the western Pütürge segment at 5 and 10 km, which had not experienced rupture during the 2020 Sivrice earthquake or the 2023 Pazarcık earthquake, as well as in the southern segment of the Malatya fault and the central segments of the EAFZ (Fig. 7). Additionally, Över et al. (2023) suggested that the Pazarcık earthquake resulted in increased stress on the Sürgü-Çardak fault, with notable stress enhancements observed at the eastern end of the Sürgü fault extending toward Malatya.

Analysis of the epicenter distribution maps indicates a notable reduction in the number of earthquakes in the region between Malatya and Kale (specifically between longitudes 38.4° and 38.6° in Fig. 2), coinciding with a significant increase in *b*-values and a decrease in stress values (Fig. 6a and 9a). This pattern may suggest the presence of a barrier structure in the area. It is well established that Cretaceous volcanics and granitoids are widespread in the northeast of the study area (MTA 2016), as highlighted by the white ellipse in Fig. 10 a and b Büyüksaraç et al. (2024) delineated the boundaries of this geological structure by employing horizontal derivative transformation techniques applied to reduced pole magnetic anomalies. The findings implied that these volcanic formations not only contribute to the segmentation of the EAFZ in the SW of Elazığ but also serve as a barrier along the western side of the volcanic between Malatya and Kale (Fig. 10c). Moreover, the epicenter of the Kale earthquake further supports the notion of a barrier, as it is located outside the proposed barrier zone. This observation strengthens the suggestion that volcanic and granitoid formations play a crucial role in shaping seismic behavior and influencing the distribution of seismic activity.

The findings of the current study also indicate positive stress changes (please see Figs. 7 and 8) associated with potential fault oriented toward the city center of Malatya, with areas of positive stress forming an arc that extends over the city (dashed line in Fig. 10d). The arc closely aligns with the border of the Malatya Plain, encompassing both the city center and the Malatya Mountains. Such linear features are commonly associated with normal faults, similar to those observed in the Bursa Plain and Uludağ Mountain (Seyitoğlu et al. 2024). Therefore, further geological investigations aimed at identifying fault traces, along with geophysical studies focusing on lateral discontinuities, will be essential for a comprehensive understanding of Malatya's tectonic framework. Also, the unnamed fault near Kale may represent a segment of a potentially active fault that is segregated by the aforementioned barrier (Fig. 10c and d). This situation draws parallels to observations made by Ateş et al. (2008) regarding the Marmara Sea region, where it was suggested that granitic intrusions act as a factor inhibiting the westward propagation of the NAFZ.

Furthermore, the *b*-values calculated for Region 2 are notably low in the northeast direction along the EAFZ. The Coulomb stress results corroborate this observation, revealing the presence of dominant positive stress lobes across all depth levels from 0 to 20 km. These findings highlight the critical need to focus on the potential for future seismic activity in the S-SE of Kale and within the Pütürge segment of the region. The alignment of positive stress distribution in the NE direction along the EAFZ appears to be associated with the Pütürge segment, extending further in an N-NE direction toward Kale. Additionally, the Coulomb stress variation map derived from the Kale earthquake specifically indicates positive stress distributions that are particularly aligned with the aftershocks occurring in both the NE and SW directions.

Conclusions

The MW 5.9 Kale earthquake (Malatya) on October 16, 2024, was investigated through a statistical assessment approach in this paper that utilized seismotectonic parameters. This analysis included the calculation of the *b*-value derived from the Gutenberg-Richter (G-R) relationship based on a dataset of 14,549 earthquakes with magnitudes (MW) $\geq$ 1.0 occurring between 1905 and 2024 within the study region. Additionally, the study examined the Coulomb stress variations associated with the aftershocks of the February 2023 earthquake sequence leading up to the Kale earthquake, as well as the Coulomb stress variation related to the Kale earthquake itself.

The outcomes are as follows:

1. The Pütürge segment of the East Anatolian Fault Zone is a major contributing factor to the Kale earthquake, as evidenced by the low *b*-values observed throughout the Erkenek and Pütürge segments. Also, the stress transfer occurring through the Pütürge segment toward the unnamed fault is attributed to the positive stress fields present in this area, indicating heightened seismic potential.
2. The positive Coulomb stress variations may be associated with a potential fault oriented toward the city center of Malatya, forming an arc that extends over the city. This estimation highlights the need for further investigation, which will be conducted in future studies utilizing more current seismological data and field observations. Such efforts will aim to provide reliable mapping and dating of the fault structure.
3. The distribution of earthquakes around Malatya, extending toward Kale, indicates a notable reduction in seismic activity. This reduction may be attributed to a possible barrier structure, consistent with findings from previous studies conducted in the area. Understanding this barrier is crucial for assessing seismic risk and fault dynamics in the region.
4. The Coulomb stress variations resulting from the Kale earthquake present significant indications of potential future seismic events in both the northeast and southwest directions of Kale. This reinforces the importance of continuous monitoring and analysis of stress distribution in order to anticipate and mitigate the risks associated with future earthquakes.

The analysis suggests a need for higher spatial resolution geological and geophysical data sets. This enhancement is crucial for accurately investigating earthquake hazards, particularly in and around the city center of Malatya. Implementing such detailed data will facilitate more precise seismic risk estimations. Additionally, it will support the development of earthquake-resistant settlement areas through urban-scale preparations. A comprehensive approach will contribute to improved safety and resilience in urban planning and infrastructure development.

Author contributions Mustafa Senkaya: Conceptualization, Investigation, Formal analysis, Resources, Writing—review & editing, Supervision. Serkan Öztürk: Conceptualization, Methodology, Investigation, Software, Formal analysis, Resources, Writing—review & editing. Hamdi Alkan: Methodology, Software, Formal analysis, Investigation, Writing—review & editing, Visualization. Aydın Büyüksaraç: Methodology, Investigation, Resources, Writing—review & editing.

Funding Open access funding provided by the Scientific and Technological Research Council of Türkiye (TÜBİTAK). No funding was received to assist with the preparation of this manuscript.

Data availability Earthquake catalogs are available at Tan (2021) for the period between 1900 and 2019. The earthquakes from 2019 to 2024 were taken from Bogazici University, Kandilli Observatory and Research Institute (KOERI, www.koeri.boun.edu.tr/sismo/zeqdb/). Also, for the focal mechanism of earthquakes, the catalog information (dip, strike, rake, etc.) was provided by AFAD) www.afad.gov.tr).

Declarations

Conflict of interest The authors declare no competing interests.

References

AFAD (2024a) 6 February 2023 01:17 Mw7.7 Earthquake. https://tadas.afad.gov.tr/event-detail/17966. Accessed 17 Apr 2024

AFAD (2024b) 6 February 2023 10:24 Mw7.6 Earthquake. https://tadas.afad.gov.tr/event-detail/17969. Accessed 17 Apr 2024

AFAD (2024c) Kale Earthquake. https://tadas.afad.gov.tr/event-detail/32756. Accessed 16 Nov 2024

AFAD (2025) AFAD - TADAS. https://tadas.afad.gov.tr/list-event. Accessed 26 Dec 2023

Akar F (2024) Spatio-temporal changes in b-value associated with the 2023 Türkiye earthquake. J Earth Syst Sci 133:185. https://doi.org/10.1007/s12040-024-02398-w

Akbaş B, Akdeniz N, Aksay A, Altun İE, Balcı V, Bilginer E, Bilgiç T, Duru M, Ercan T, Gedik İ, Günay Y, Güven İH, Hakyemez HY, Konak N, Papak İ, Pehlivan Ş, Sevin M, Şenel M, Tarhan N, Turhan N, Türkecan A, Ulu Ü, Uğuz MF, Yurtsever AT (2011) 1:1.250.000 scaled Geological map of Turkey.General Directorate of Mineral Research andExploration Publication, Ankara, Turkey

Akgün E (2024) Kinematic and morphometric evidence for recent reactivation of the Kale-Yeşilyurt fault zone within the East Anatolian fault system. J Mt Sci 21:4149–4176. https://doi.org/10.1007/s11629-024-9251-2

Akgün E, Topal S, Softa M et al (2025) Evidence for an aseismic gap between the Mw6.8 Pütürge (Elazığ) and 7.8 Pazarcık (Kahramanmaraş) earthquakes in the east Anatolian fault system,

southeast Türkiye. J Struct Geol 190:105293. https://doi.org/10.1016/j.jsg.2024.105293
Aki K (1965) A note on the use of microseisms in determining the shallow structures of the earth's crust. Geophysics 30:665–666. https://doi.org/10.1190/1.1439640
Ali SM, Abdelrahman K (2023) The impact of fractal dimension, stress tensors, and earthquake probabilities on seismotectonic characterisation in the red Sea. Fractal and Fraction 7:658. https://doi.org/10.3390/fractalfract7090658
Alkan H, BÜYÜKSARAÇBektaş AO (2024) Investigation of earthquake sequence and stress transfer in the Eastern Anatolia Fault Zone by Coulomb stress analysis. Turk J Earth Sci 33:56–68
Alkan H, Öztürk S, Akkaya İ (2023) Seismic Hazard Implications in and Around the Yedisu Seismic Gap (Eastern Türkiye) Based on Coulomb Stress Changes, b-Values, and S-wave Velocity. Pure Appl Geophys 180:3227–3248. https://doi.org/10.1007/s00024-023-03342-7
Ansari S (2016) Co-seismic stress transfer and magnitude-frequency distribution due to the 2012 Varzaqan-Ahar earthquake doublets (Mw 6.5 and 6.4), NW Iran. J Asian Earth Sci 132:129–137. https://doi.org/10.1016/j.jseaes.2016.10.006
Ates A, Bilim F, Buyuksarac A, Bektas Ö (2008) A tectonic interpretation of the Marmara Sea, NW Turkey from geophysical data. Earth Planet Sp 60:169–177. https://doi.org/10.1186/BF03352780
Balkaya M, Akyüz HS, Özden S (2023) Paleoseismology of the Sürgü and Çardak faults - splays of the Eastern Anatolian Fault Zone, Türkiye. Turkish Journal of Earth Sciences 32:402–420. https://doi.org/10.55730/1300-0985.1851
Bayrak E, Yılmaz Ş, Softa M et al (2015) Earthquake hazard analysis for East Anatolian Fault Zone, Turkey. Nat Hazards 76:1063–1077. https://doi.org/10.1007/s11069-014-1541-5
Büyüksaraç A, Bektaş Ö, Alkan H (2024) Fault modeling around southern Anatolia using the aftershock sequence of the Kahramanmaraş earthquakes (Mw = 7.7 and Mw = 7.6) and an interpretation of potential field data. Acta Geophys 72:2985–2996. https://doi.org/10.1007/s11600-023-01192-4
Console R, Montuori C, Murru M (2000) Statistical assessment of seismicity patterns in Italy: Are they precursors of subsequent events? J Seismolog 4:435–449. https://doi.org/10.1023/A:1026540018598
Dai X, Liu X, Liu R et al (2024) Coseismic slip distribution and coulomb stress change of the 2023 MW 7.8 Pazarcik and MW 7.5 Elbistan earthquakes in Turkey. Remote Sensing 16:240. https://doi.org/10.3390/rs16020240
Emre Ö, Duman TY, Özalp S et al (2018) Active fault database of Turkey. Bull Earthquake Eng 16:3229–3275. https://doi.org/10.1007/s10518-016-0041-2
Erdik M, Alpay BY, Onur T et al (1999) Assessment of earthquake hazard in Turkey and neighboring regions. Ann Geofis 42:1125–1138. https://doi.org/10.4401/ag-3773
Frohlich C, Davis SD (1993) Teleseismic b values; Or, much ado about 1.0. J Geophys Res: Solid Earth 98:631–644. https://doi.org/10.1029/92JB01891
Gabriel A, Ulrich T, Marchandon M et al (2023) 3D dynamic rupture modeling of the 6 February 2023, Kahramanmaraş, Turkey Mw 7.8 and 7.7 Earthquake Doublet Using Early Observations. The Seismic Record 3:342–356. https://doi.org/10.1785/0320230028
Gokceoglu C, Karahan S (2023) Seismic Performance of Transportation Tunnels in the Region Affected by the 6 February 2023 Türkiye Earthquake Sequence: A General Assessment□□□□□□□□□□□□□
Gutenberg B, Richter CF (1944) Frequency of earthquakes in California*. Bull Seismol Soc Am 34:185–188. https://doi.org/10.1785/BSSA0340040185
Holliday JR, Chen C, Tiampo KF et al (2007) A RELM earthquake forecast based on pattern informatics. Seismol Res Lett 78:87–93. https://doi.org/10.1785/gssrl.78.1.87
Jia Z, Jin Z, Marchandon M et al (2023) The complex dynamics of the 2023 Kahramanmaraş, Turkey, Mw 7.8-7.7 earthquake doublet. Science 381:985–990. https://doi.org/10.1126/science.adi0685
Karabacak V, Özkaymak Ç, Sözbilir H et al (2023) The 2023 Pazarcık (Kahramanmaraş, Türkiye) earthquake (Mw 7.7): implications for surface rupture dynamics along the East Anatolian Fault Zone. J Geol Soc 180:2023–3020. https://doi.org/10.1144/jgs2023-020
King GCP, Stein RS, Lin J (1994) Static stress changes and the triggering of earthquakes. Bull Seismol Soc Am 84:935–953. https://doi.org/10.1785/BSSA0840030935
KOERI (2023) Bogaziçi University Kandilli Observatory and Earthquake Research Institute. http://www.koeri.boun.edu.tr/sismo/2/deprem-bilgileri/buyuk-depremler/. Accessed 2 Oct 2023
Köküm M (2024) Kinematic and dynamic fault slip analyses: Implications from the surface rupture of the 2023 Elbistan (Kahramanmaraş) (Mw7.6) earthquake. Türkiye. Journal of Structural Geology 187:105235. https://doi.org/10.1016/j.jsg.2024.105235
Li S, Wang X, Tao T et al (2023) Source model of the 2023 Turkey earthquake sequence imaged by sentinel-1 and GPS measurements: implications for heterogeneous fault behavior along the East Anatolian fault zone. Remote Sensing 15:2618. https://doi.org/10.3390/rs15102618
Liang P, Xu Y, Zhou X et al (2025) Coseismic surface ruptures of MW7.8 and MW7.5 earthquakes occurred on February 6, 2023, and seismic hazard assessment of the East Anatolian Fault Zone. Southeastern Türkiye Sci China Earth Sci 68:611–625. https://doi.org/10.1007/s11430-024-1457-7
Liao L, Li P, Yang J, Feng J (2022) Influence of regional background stress fields on the spontaneous rupture of the major faults around Xiluodu dam, China. Earthq Sci 35:398–409. https://doi.org/10.1016/j.eqs.2022.10.004
Lin J, Stein RS (2004) Stress triggering in thrust and subduction earthquakes and stress interaction between the southern San Andreas and nearby thrust and strike-slip faults. J Geophys Res: Solid Earth. https://doi.org/10.1029/2003JB002607
Melgar D, Taymaz T, Ganas A et al (2023) Sub- and super-shear ruptures during the 2023 Mw 7.8 and Mw 7.6 earthquake doublet in SE Türkiye. Seismica 2:12. https://doi.org/10.26443/seismica.v2i3.387
Mogi K (1962) Magnitude-frequency relation for elastic shocks accompanying fractures of various materials and some related problems in earthquakes. Bull Earthq Res Inst, Univ Tokyo 40:831–853
MTA (2016) Geoscience Mapviewer and Drawing Editor. http://yerbilimleri.mta.gov.tr/anasayfa.aspx. Accessed 2 Dec 2019
Njinju EA, Kolawole F, Stamps DS et al (2025) Intrarift fault interactions: insights from coseismic stress redistribution from large seismogenic segment ruptures, Northern Malawi Rift. J Struct Geol 191:105326. https://doi.org/10.1016/j.jsg.2024.105326
Ogata Y, Imoto M, Katsura K (1991) 3-D spatial variation of b-values of magnitude-frequency distribution beneath the Kanto District, Japan. Geophys J Int 104:135–146. https://doi.org/10.1111/j.1365-246X.1991.tb02499.x
Ormeni R, Hasimi A, Öztürk S, Çomo E (2023) Correlations between seismic b-value and heat flow density in Vlora-Lushnja-Elbasani-Dibra Fault Zone in Elbasani area, central Albania. Baltica. https://doi.org/10.5200/baltica.2023.2.7
Över S, Demirci A, Özden S (2023) Tectonic implications of the February 2023 Earthquakes (Mw7.7, 7.6 and 6.3) in south-eastern Türkiye. Tectonophysics 866:230058. https://doi.org/10.1016/j.tecto.2023.230058

Öztürk S (2020) A study on the variations of recent seismicity in and around the Central Anatolian region of Turkey. Phys Earth Planet Inter 301:106453. https://doi.org/10.1016/j.pepi.2020.106453

Öztürk S, Alkan H (2023) Multiple parameter analysis for assessing and forecasting earthquake hazards in the Lake Van region Turkey. Baltica. https://doi.org/10.5200/baltica.2023.2.4

Öztürk S, Şahin Ş (2019) A statistical space-time-magnitude analysis on the aftershocks occurrence of the July 21th, 2017 $MW = 6.5$ Bodrum-Kos, Turkey, earthquake. J Asian Earth Sci 172:443–457. https://doi.org/10.1016/j.jseaes.2018.10.008

Peikert J, Hampel A, Bagge M (2023) Three-dimensional finite-element modeling of Coulomb stress changes on normal and thrust faults caused by pore fluid pressure changes and postseismic viscoelastic relaxation. Geosphere 20:105–128. https://doi.org/10.1130/GES02672.1

Reilinger R, McClusky S, Vernant P et al (2006) GPS constraints on continental deformation in the Africa-Arabia-Eurasia continental collision zone and implications for the dynamics of plate interactions. J Geophys Res: Solid Earth. https://doi.org/10.1029/2005JB004051

Rundle JB, Tiampo KF, Klein W, Sá Martins JS (2002) Self-organization in leaky threshold systems: the influence of near-mean field dynamics and its implications for earthquakes, neurobiology, and forecasting. Proc Natl Acad Sci 99:2514–2521. https://doi.org/10.1073/pnas.012581899

Scholz CH (1968) The frequency-magnitude relation of microfracturing in rock and its relation to earthquakes. Bull Seismol Soc Am 58:399–415. https://doi.org/10.1785/BSSA0580010399

Scholz CH (2015) On the stress dependence of the earthquake b value. Geophys Res Lett 42:1399–1402. https://doi.org/10.1002/2014GL062863

Schorlemmer D, Wiemer S, Wyss M (2005) Variations in earthquake-size distribution across different stress regimes. Nature 437:539–542. https://doi.org/10.1038/nature04094

Seyitoğlu G, Esat K, Tün M et al (2024) Newly discovered, the Kayapa-Yenişehir cross-basin fault: as revealed by geological and geophysical studies along the southern branch of the north Anatolian fault Zone, a possible source of the destructive 1855 Bursa earthquakes. J Struct Geol 179:105028. https://doi.org/10.1016/j.jsg.2023.105028

Sharma V, Biswas R (2025) Seismic quiescence and *b*-value anomalies preceding the 6th February 2023 earthquake doublet (M_W 7.8, M_W 7.6) in Kahramanmaraş, Türkiye: a comprehensive analysis of seismic parameters along the East Anatolian Fault Zone. Acta Geophys 73:1159–1185. https://doi.org/10.1007/s11600-024-01443-y

Softa M, KOÇBULUT F, AKGÜN E et al (2024) Surface rupture during the 6th of February 2023 Mw 76 Elbistan-Ekinözü (Kahramanmaraş) earthquake: implications for fault rupture dynamics along the northern branch of East Anatolian Fault Zone. Turk J Earth Sci 33:1–21. https://doi.org/10.55730/1300-0985.1895

Stein RS, King GCP, Lin J (1994) Stress Triggering of the 1994 M = 6.7 Northridge, California. Earthquake by Its Predecessors Science 265:1432–1435. https://doi.org/10.1126/science.265.5177.1432

Tan O (2021) A homogeneous earthquake catalogue for Turkey. Nat Hazard 21:2059–2073. https://doi.org/10.5194/nhess-21-2059-2021

Tan O (2024) Long-term Aftershock Properties of the Catastrophic 6 February 2023 Kahramanmaraş (Türkiye) Earthquake Sequence. Acta Geophys. https://doi.org/10.1007/s11600-024-01419-y

Tatar O, Sözbilir H, Koçbulut F et al (2020) Surface deformations of 24 January 2020 Sivrice (Elazığ)–Doğanyol (Malatya) earthquake (Mw = 6.8) along the Pütürge segment of the East Anatolian Fault Zone and its comparison with Turkey's 100-year-surface ruptures. Med Geosc Rev 2:385–410. https://doi.org/10.1007/s42990-020-00037-2

Tinti S, Gasperini P (2024) The estimation of b-value of the frequency–magnitude distribution and of its 1σ intervals from binned magnitude data. Geophys J Int 238:433–458. https://doi.org/10.1093/gji/ggae159

Toda S, Stein RS, Richards-Dinger K, Bozkurt SB (2005) Forecasting the evolution of seismicity in southern California: animations built on earthquake stress transfer. J Geophys Res: Solid Earth 110:12. https://doi.org/10.1029/2004JB003415

Toda S, Lin J, Stein RS (2011) Using the 2011 Mw 9.0 off the Pacific coast of Tohoku Earthquake to test the Coulomb stress triggering hypothesis and to calculate faults brought closer to failure. Earth Planet Sp 63:725–730. https://doi.org/10.5047/eps.2011.05.010

Utsu T (1971) Aftershock and earthquake statistic (III): Analyses of the distribution of earthquakes in magnitude, time and space with special consideration to clustering characteristics of earthquake occurrence. Journal of the Faculty of Science, Hokkaido University Series VII:379–441

Wan Y, Shen Z-K (2010) Static Coulomb stress changes on faults caused by the 2008 Mw 7.9 Wenchuan. Chin Earthquake Tectonophys 491:105–118. https://doi.org/10.1016/j.tecto.2010.03.017

Whitney DL, Delph JR, Thomson SN et al (2023) Breaking plates: creation of the East Anatolian fault, the Anatolian plate, and a tectonic escape system. Geology 51:673–677. https://doi.org/10.1130/G51211.1

Wiemer S (2001) A software package to analyze seismicity: ZMAP. Seismol Res Lett 72:373–382. https://doi.org/10.1785/gssrl.72.3.373

Wiemer S, Katsumata K (1999) Spatial variability of seismicity parameters in aftershock zones. J Geophys Res: Solid Earth 104:13135–13151. https://doi.org/10.1029/1999JB900032

Wiemer S, Wyss M (2000) Minimum magnitude of completeness in earthquake catalogs: examples from Alaska, the Western United States, and Japan. Bull Seismol Soc Am 90:859–869. https://doi.org/10.1785/0119990114

Yadav RBS, Gahalaut VK, Chopra S, Shan B (2012) Tectonic implications and seismicity triggering during the 2008 Baluchistan, Pakistan earthquake sequence. J Asian Earth Sci 45:167–178. https://doi.org/10.1016/j.jseaes.2011.10.003

Yang L, Wang J, Xu C (2024) Coseismic Coulomb stress changes induced by a 2020–2021 MW > 7.0 Alaska earthquake sequence in and around the Shumagin gap and its influence on the Alaska-Aleutian subduction interface. Geodesy and Geodyn 15:1–12. https://doi.org/10.1016/j.geog.2023.04.007

Yolsal-Çevikbilen S, Taymaz T, Irmak TS et al (2024) Source geometry and rupture characteristics of the 20 February 2023 Mw 6.4 Hatay (Türkiye) Earthquake at Southwest edge of the East Anatolian Fault. Geochem, Geophys, Geosyst 25:2023011353. https://doi.org/10.1029/2023GC011353

Zhao J-J, Chen Q, Yang Y-H, Xu Q (2023) Coseismic faulting model and post-seismic surface motion of the 2023 Turkey-Syria Earthquake doublet revealed by InSAR and GPS measurements. Remote Sensing 15:3327. https://doi.org/10.3390/rs15133327